Chapter 5

Aminoacid-derivatized Cu (II) complexes: Synthesis, DNA interactions and *in vitro* Cytotoxicity.

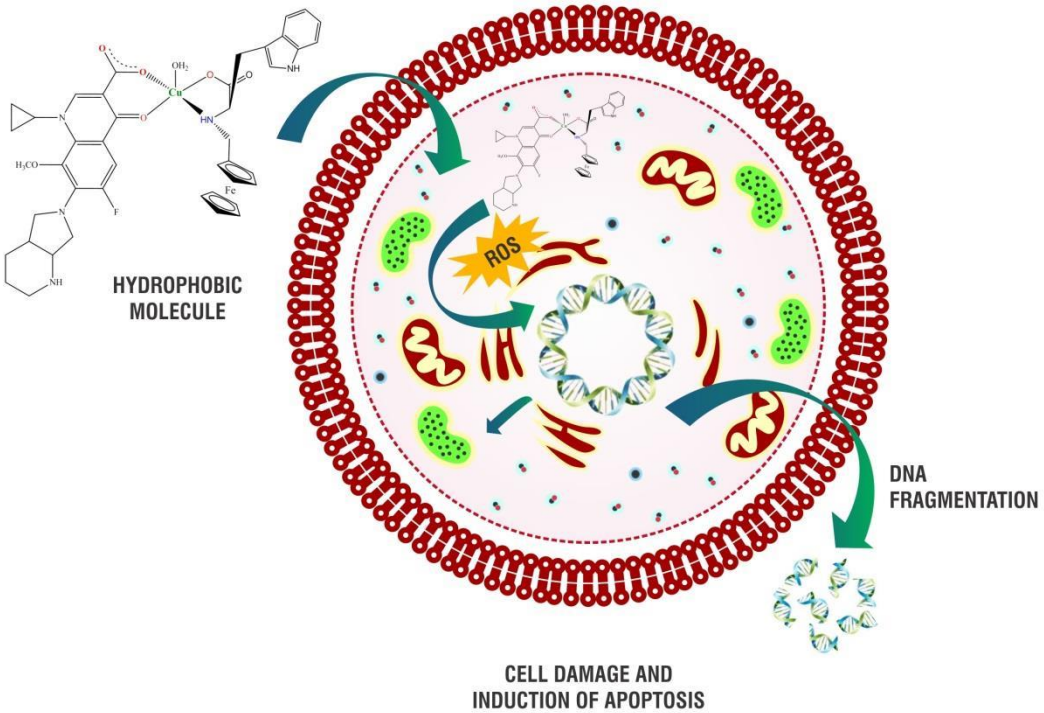

5.1 Introduction

Medicinal inorganic chemistry offers additional opportunities for the design of therapeutic agents not accessible to organic compounds [1–3]. The wide range of coordination numbers and geometries, available redox states, thermodynamic and kinetic characteristics, and intrinsic properties of the cationic metal ion and ligand itself offer the medicinal chemist a large variety of reactivities to be exploited.

The widespread success of cisplatin in the clinical treatment of various types of neoplasias has placed metal-based drugs in the frontline in the fight against cancer [1,4]. Although highly effective in treating a variety of cancers, the cure with cisplatin is still limited by dose-limiting side effects [5] and inherited or acquired resistance phenomena, only partially amended by employment of new platinum drugs [6–9]. These problems have stimulated an extensive search and prompted chemists to develop alternative strategies, based on different metals, with improved pharmacological properties and aimed at different targets [10].

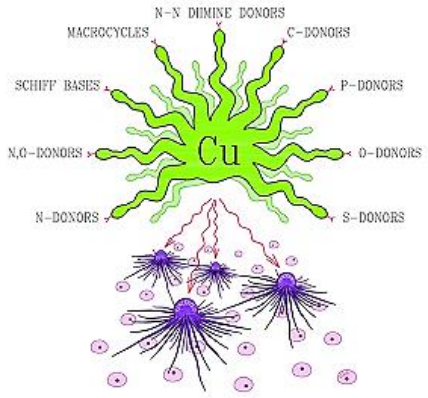

Source: Carlo Santin *et* al Chem. Rev.2014, 114, 815–862

In this field, copper complexes showed encouraging perspectives [11–15]. Copper-based complexes have been investigated on the assumption that endogenous metals may be less toxic for normal cells with respect to cancer cells. However, copper can also be toxic due to its redox activity and affinity for binding sites that should be occupied by other metals. The altered metabolism of cancer cells

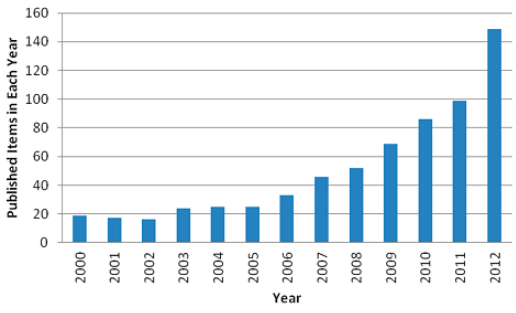

Fig 5.1. No. of aricles *in web of Science* on the topic of " copper and anticancer from 2000 to 2012.

and differential response between normal and tumor cells to copper are the basis for development of copper complexes endowed with antineoplastic characteristics (Fig 5.1). Copper is an essential element for most aerobic organisms, employed as a structural and catalytic cofactor, and consequently it is involved in many biological pathways [16]. Taking this into account, much attention has been given to research on the mechanisms of absorption, distribution, metabolism, and excretion of copper, as well as on its therapeutic role in development of cancer and other diseases [11].

In the field of bioorganometallic chemistry, derivatives of ferrocene exhibit a variety of medicinal properties by serving as antibacterial, antimalarial and antitumor agents [17]. The ability of ferrocenyl compounds to cleave DNA may be responsible for these diverse properties [17–19]. While a multitude of ferrocenyl compounds, exist, we are most interested in the design of ferrocenyl amino acids which have been developed mainly for use in biomedical studies [19]. Ferrocenylated amino acids have been intensely studied in the recent past as redox-active biomolecular probes and structural models for peptides [20]. Recently, in vivo techniques to genetically encode for site-specific incorporation of unnatural redox active amino acids (containing ferrocenyl groups) into proteins have been developed [21-23] to study electron transfer activity [24].

The ferrocene derivatives among the metallocenes are of importance for their stability in a biological medium and for their lipophilic, nontoxic, and reversible redox properties [25,26]. The cyclopentadienyl rings of ferrocene could be suitably functionalized, and ferrocenyl derivatives are known to exhibit antitumor, antimalarial, and antifungal properties. For example, the ferrocenyl moiety (Fc) in ferrocifen, the ferrocene-appended anticancer drug tamoxifen, makes the drug effective against both hormone-independent (ER-) and hormone-dependent (ER+) cells [27]. Similarly, ferroquine, the ferrocene-attached antimalarial drug chloroquine, is more effective than chloroquine. [28]

Transition metal based organometallic compounds have excellent biological activity, and such compounds are potent therapeutics for cancer, malaria, as radiopharmaceuticals and antibiotics. Transition metals are particularly suitable for this purpose because they can adopt a wide variety of coordination numbers, geometries and oxidation states in comparison with carbon and other main group elements [29]. A further reason for using metal containing compounds as structural scaffolds relates to the kinetic stabilities of their coordination spheres in the biological environment [30]. Investigation of the interactions of DNA with small molecules can serve as a foundation for the design of new types of pharmaceutical molecules. The development of interaction models and the elucidation of the mechanisms of interaction of transition metal complexes with DNA and their subsequent applications in molecular biology continue to attract significant attention. In particular, considerable interest has been generated in DNA binding and DNA cleavage by redox and photoactive metal complexes in order to explore the sequence specificities of DNA binding using a variety of intercalating ligands [31–33]. Moreover, certain metal complexes have been shown to be capable of cleaving DNA strands. In the case of cancer genes, the cleavage of the DNA double strands can destroy their replication ability.

The foregoing facts stimulated our interest in the syntheses, structure, DNA binding, DNA cleavage and anticancer properties of mixed ligand Cu complexes. Amino acid conjugated ferrocene and benzaldehyde mannich bases and their ternary copper complexes with MFL were synthesized. The structures of the new complexes were established on the basis of spectroscopic and electrochemical data. In addition, DNA cleavage abilities and anticancer activities of the complexes have been rationalized in terms of their DNA binding affinity. All the complexes showed strong affinity to bind to DNA, induce apoptosis and were good antitumor agents in a dose & time dependent manner.

5.2 General synthesis of complexes

(A) Synthesis of Ligands: **L1-L4**

The amino acids (5.0 mmol) and NaOH (0.2 g, 5.0 mmol) in dry methanol (10 mL) were stirred for 30 min to get a homogeneous solution. A methanol solution (10 mL) of ferrocenecarboxaldehyde (1.07 g, 5.0 mmol) was added dropwise to the above solution, which was refluxed for 90 min, cooled, and treated with sodium borohydride (0.38 g, 10.o mmol) with constant stirring. The solvent was evaporated, the resulting mass was dissolved in water and acidified with dilute HCl, and the solution pH was maintained at 5.6. The ligands that precipitated as a yellow solids were filtered, thoroughly washed with water and cold methanol, and finally dried in vacuum over P_4O_{10}.

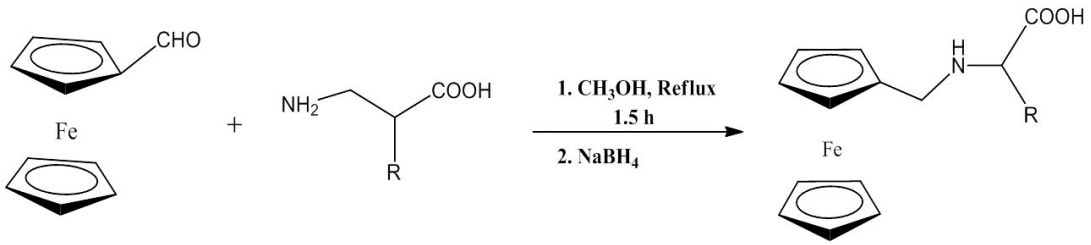

Ferrocene Carboxyaldehyde **Amino acid** **Ferrocenyl mannich base L1-L4**

-R	Amino acid	Ligand	Complex
CH_2(3-indoyl)	Tryptophan	L1	C1
-CH_2Ph	Phenyl alanine	L2	C2
-$CH_2CH(CH_3)_2$	Leucine	L3	C3
-CH_2(4-hydroxyphenyl)	Tyrosine	L4	C4

Scheme 5.1

(B) Synthesis of Ligands: L5-L8

The amino acids (2.0 mmol) were initially dissolved in dry methanol (20 mL) with addition of NaOH (0.08 g, 2.0 mmol) and continuous stirring. Benzaldehyde (0.2 mL, 2.0 mmol) was subsequently added to the above solution. The mixture was refluxed for 1 h, cooled, and then treated with an excess of solid $NaBH_4$ with constant stirring. After stirring for ~15 min, the solvent was removed on rotary evaporator and the resulting mass was dissolved in water followed by treatment with dilute HCl to maintain a pH of ~5.5. White solids thus precipitated were filtered off, thoroughly washed with water and cold methanol, and finally dried in vacuum over P_4O_{10}.

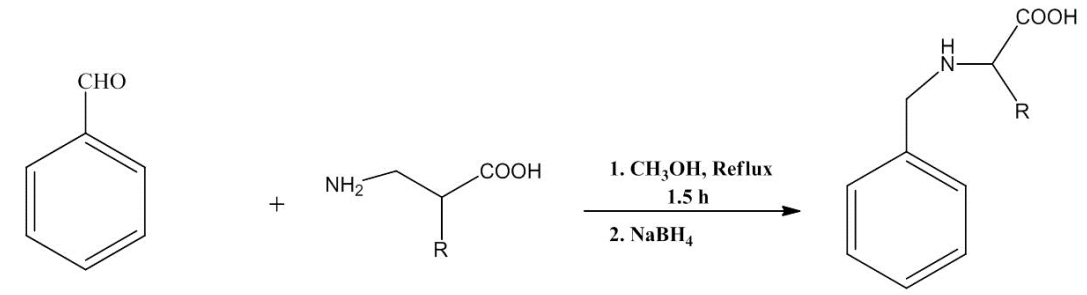

Benzaldehyde **Amino acid** **Mannich base L5-L8**

-R	Amino acid	Ligand	Complex
CH_2(3-indoyl)	Tryptophan	L5	C5
-CH_2Ph	Phenyl alanine	L6	C6
-$CH_2CH(CH_3)_2$	Leucine	L7	C7
-CH_2(4-hydroxyphenyl)	Tyrosine	L8	C8

Scheme 5.2

(C) Synthesis of Complexes: C1-C8

Complexes **1-8** were prepared by a general synthetic procedure in which (1.0 mmol) quantity of copper(II) acetate in 15 mL of methanol was reacted with moxifloxacin

(MFL, 1.0 mmol) while stirring at room temperature for 0.5 h followed by addition of solid **L1-L8** (1.0 mmol) in small portions with continuous stirring (Scheme 5.3 and 5.2). The reaction mixture was stirred for 2 h, and the product isolated as green solids in~75% yield. The solid was isolated, washed with water and cold methanol, and finally dried in vacuum over P_4O_{10}.

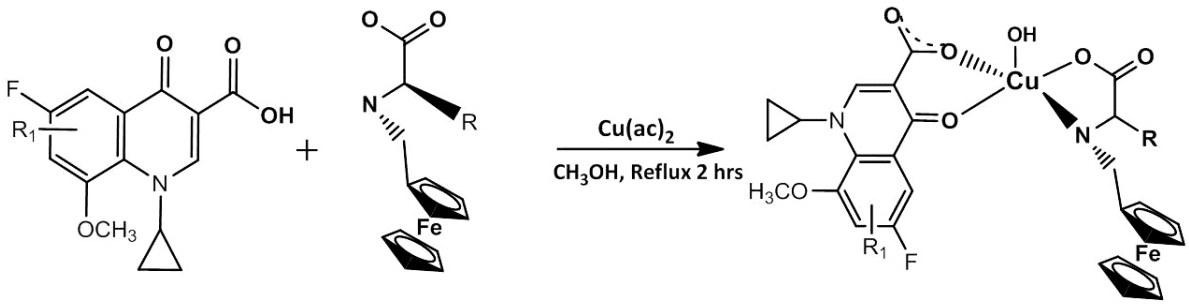

Moxifloxacin **Mannich Base L1-L4** **Cu-Complex C1-C4**

Scheme 5.3

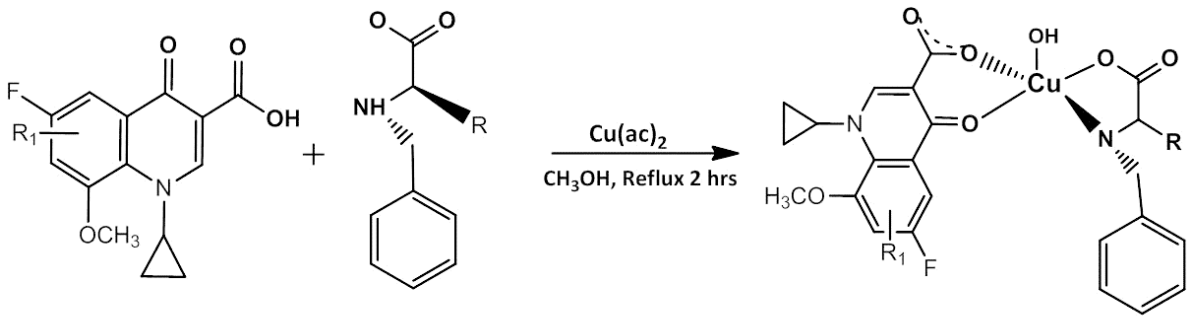

Moxifloxacin **Mannich Base L5-L8** **Cu-Complex C5-C8**

Scheme 5.4

5.3 Physicochemical data of the synthesized Ligands & Complexes

A. **(L1)**

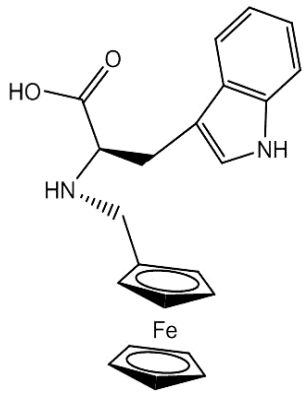	Yield: 81 % Molecular weight: 402.1 g/mol Molecular formula: $C_{22}H_{22}FeN_2O_2$ Calc. (%): C, 65.69; H, 5.51; N, 6.96; Fe, 13.88 Found (%):C, 65.54; H, 5.48; N, 7.10; Fe, 13.52 λ_{max}: 207 nm. ESI-MS [MeOH, *m/z*]: 402.2 [M^+]

B. **(L2)**

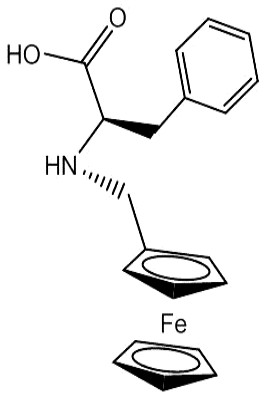	Yield: 87% Molecular weight: 368.27 g/mol Molecular formula: $C_{20}H_{26}FeNO_2$ Calc. (%): C, 65.23; H, 7.12; N, 3.80; Fe, 15.16 Found (%):C, 64.98; H, 7.10; N, 3.59; Fe, 15.88 λ_{max}: 209 nm. ESI-MS [MeOH, *m/z*]: 369.0 [M+1]

C. **(L3)**

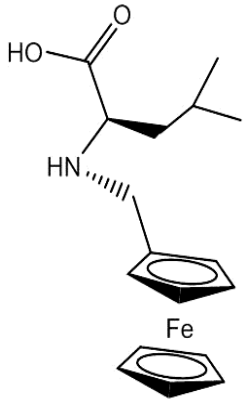	Yield: 76% Molecular weight: 334.15 g/mol Molecular formula: $C_{17}H_{28}FeNO_2$ Calc. (%): C, 61.09; H, 8.44; N, 4.19; Fe, 16.71 Found (%):C, 60.89; H, 8.38; N, 4.10; Fe, 16.52 λ_{max}: 208 nm. ESI-MS [MeOH, *m/z*]: 335.1 [M+1]

D. **(L4)**

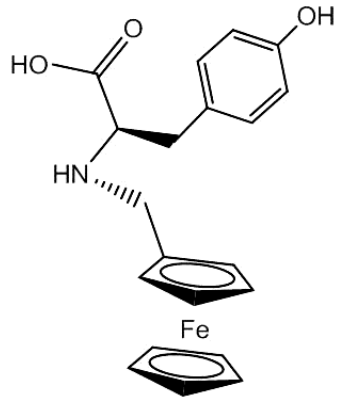	Yield: 86 % Molecular weight: 379.09 g/mol Molecular formula: $C_{20}H_{21}FeNO_3$ Calc. (%): C, 63.34; H, 5.58; N, 3.69; Fe, 14.73 Found (%):C, 63.24; H, 5.48; N, 3.50; Fe, 14.70 λ_{max}: 208 nm. ESI-MS [MeOH, *m/z*]: 378.2[M-1]

E. 2-(benzylamino)-3-(1H-indol-3-yl)propanoic acid **(L5)**

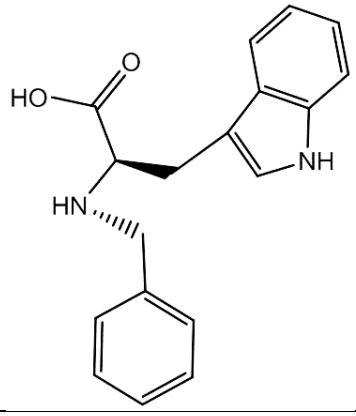	Yield: 75 % Molecular weight: 294.35 g/mol Molecular formula: $C_{28}H_{28}N_2O_2$ Calc. (%): C, 73.45; H, 6.61; N, 9.52 Found (%):C, 73.58.54; H, 6.50; N, 9.57 λ_{max}: 280 nm. ESI-MS [MeOH, *m/z*]: 295.1 [M+1]

F. 2-(benzylamino)-3-phenylpropanoic acid **(L6)**

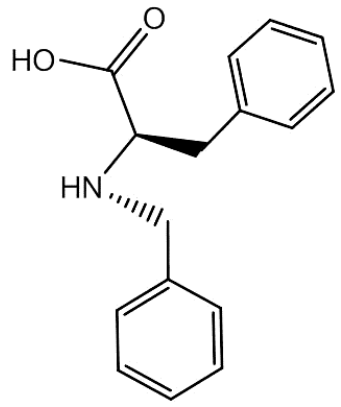	Yield: 82% Molecular weight: 522.31 g/mol Molecular formula: $C_{26}H_{17}NO_2$ Calc. (%): C, 75.27; H, 6.71; N, 5.49 Found (%):C, 74.98; H, 6.82; N, 5.48 λ_{max}: 258, 323 nm. ESI-MS [MeOH, *m/z*]: 522.1 [M^+]

G. 2-(benzylamino)-4-methylpentanoic acid **(L7)**

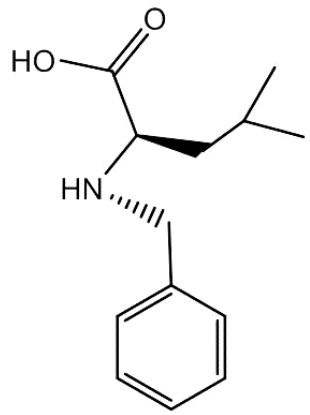	Yield: 84 % Molecular weight: 221.13 g/mol Molecular formula: $C_{13}H_{19}NO_2$ Calc. (%): C, 70.56; H, 8.65; N, 6.33 Found (%):C, 70.0 ; H, 8.62; N, 6.45 λ_{max}: 257.6, 261 nm. ESI-MS [MeOH, *m/z*]: 220.1 [M-1]

H. 2-(benzylamino)-3-(4-hydroxyphenyl)propanoic acid **(L8)**

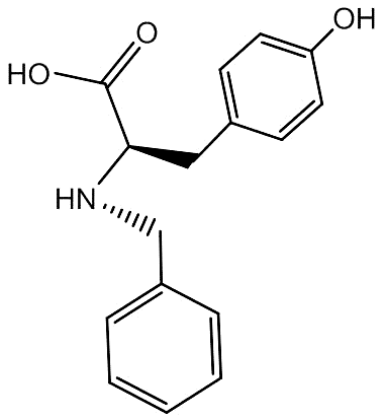	Yield: 78% Molecular weight: 271.3 g/mol Molecular formula: $C_{16}H_{17}NO_3$ Calc. (%): C, 70.83; H, 6.32; N, 5.16 Found (%):C, 69.94; H, 6.32; N, 5.10 λ_{max}: 218, 276 nm. ESI-MS [MeOH, *m/z*]: 271.3 [M^+]

Structure of Complexes:

I. [Cu(MFL)(L1)H_2O] **(C1)**

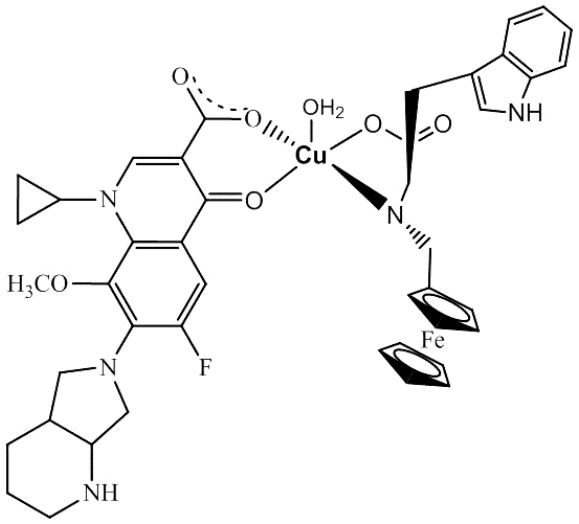

Yield: 68%
Molecular weight: 883.24 g/mol
Molecular formula: $C_{43}H_{46}CuFFeN_5O_7$
Calc. (%): C, 58.47; H, 5.25; N, 6.32; Cu, 7.19
Found (%):C, 58.42; H, 5.18; N, 6.30; Cu, 7.15
λ_{max}: 289, 339 nm.
ESI-MS [MeOH, *m/z*]: 883.3 [M^+]

J. [Cu(MFL)(L2)H_2O] **(C2)**

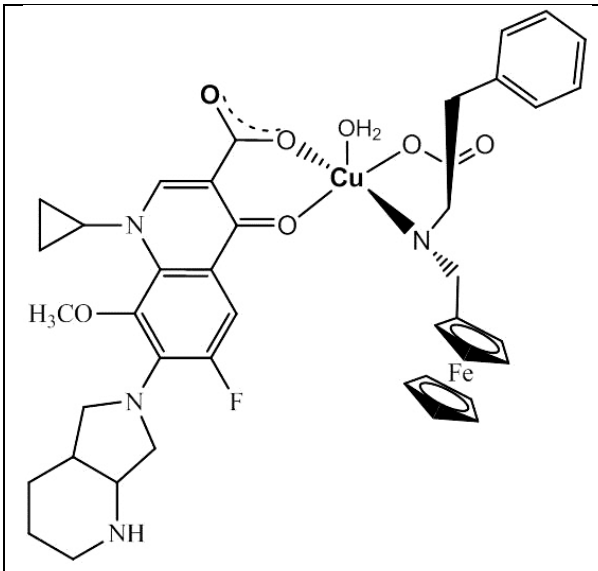

Yield: 72%
Molecular weight: 844.21 g/mol
Molecular formula: $C_{41}H_{45}CuFFeN_4O_7$
Calc. (%): C, 58.33; H, 5.37; N, 6.62; Cu, 7.53
Found (%):C, 58.55; H, 5.38; N, 6.70; Cu, 7.50
λ_{max}: 290, 338 nm.
ESI-MS [MeOH, *m/z*]: 842.2 [M-2]

K. [Cu(MFL)(L3)H_2O] **(C3)**

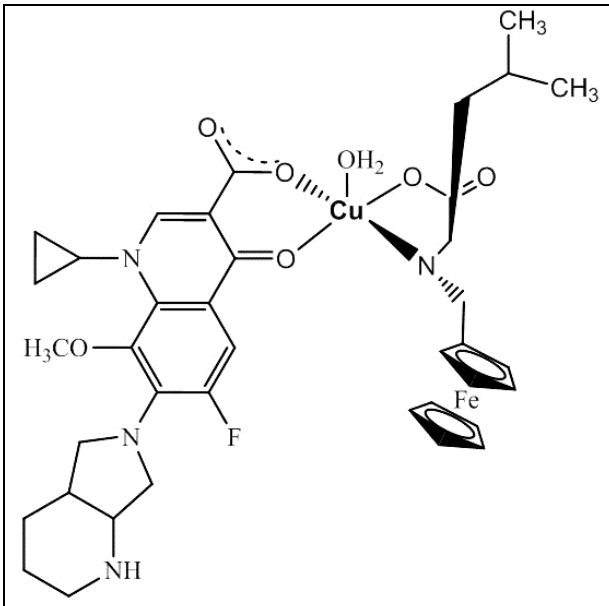

Yield: 68%
Molecular weight: 810.19 g/mol
Molecular formula: $C_{38}H_{47}CuFFeN_4O_7$
Calc. (%): C, 56.33; H, 5.85; N, 6.92;Cu, 7.84
Found (%):C, 56.50; H, 5.79; N, 6.96; Cu, 7.80
λ_{max}: 290, 239 nm.
ESI-MS [MeOH, *m/z*]: 810.0 [M^+]

L. [Cu(MFL)(L4)H_2O] **(C4)**

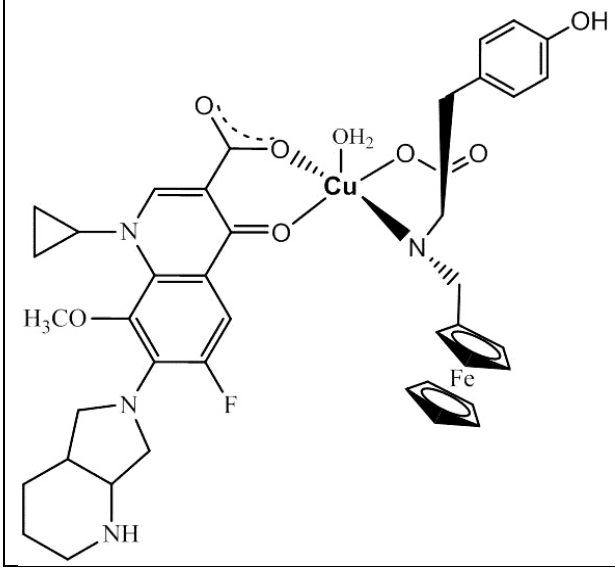

Yield: 65%
Molecular weight: 859.19 g/mol
Molecular formula: $C_{41}H_{45}CuFFeN_4O_8$
Calc. (%): C, 65.69; H, 5.51; N, 6.96; Cu, 7.39
Found (%):C, 65.54; H, 5.48; N, 7.10; Cu, 7.40
λ_{max}: 287, 339 nm.
ESI-MS [MeOH, *m/z*]: 587.9 [M-2]

M. [Cu(MFL)(L5)H_2O] **(C5)**

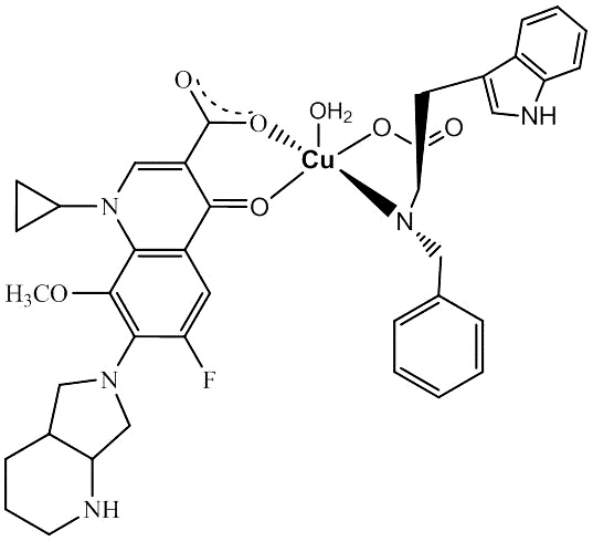

Yield: 63%
Molecular weight: 775.24 g/mol
Molecular formula: $C_{39}H_{43}CuFN_5O_7$
Calc. (%): C,60.34; H, 5.58; N, 9.02; Cu, 8.19
Found (%):C, 60.14; H, 5.57; N, 9.10; Cu, 8.15
λ_{max}: 290, 338 nm.
ESI-MS [MeOH, *m/z*]: 774.40 [M-1]

N. [Cu(MFL)(L6)H_2O] **(C6)**

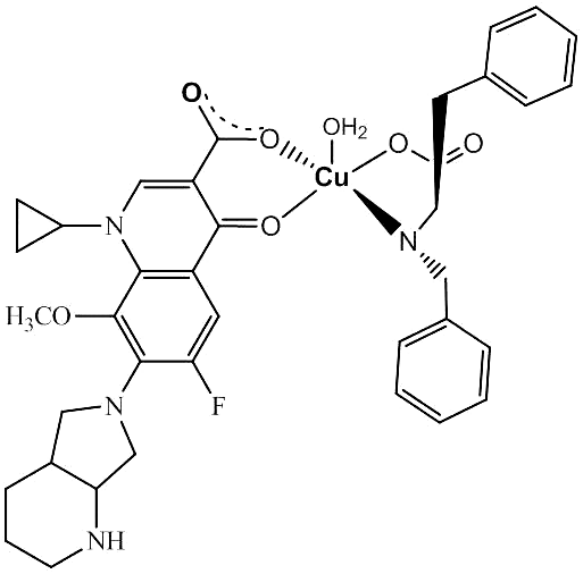

Yield: 64%
Molecular weight: 736.23 g/mol
Molecular formula: $C_{37}H_{42}CuFN_4O_7$
Calc. (%): C, 60.27; H, 5.74; N, 7.60; Cu, 8.62
Found (%):C, 60.21; H, 5.69; N, 7.59; Cu, 8.61
λ_{max}: 289, 337 nm.
ESI-MS [MeOH, *m/z*]: 737.4 [M+1]

O. [Cu(MFL)(L7)H_2O] **(C7)**

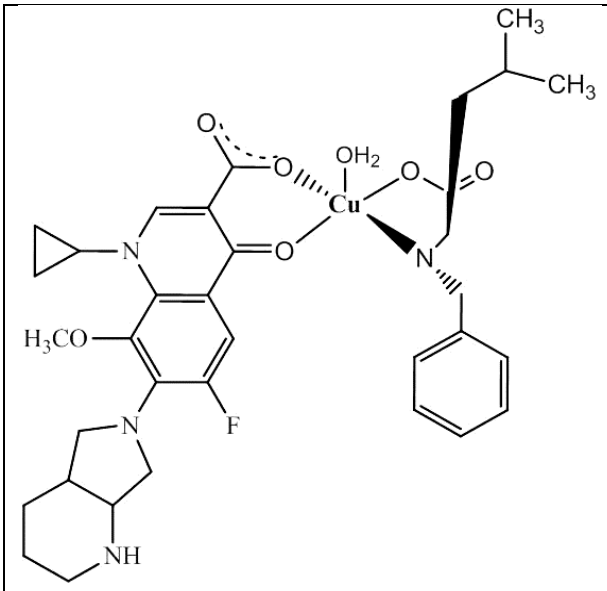

Yield: 70%
Molecular weight: 702.23 g/mol
Molecular formula: $C_{34}H_{44}CuFN_4O_7$
Calc. (%): C, 58.07; H, 6.31; N, 7.97; Cu, 9.04
Found (%):C, 58.02; H, 6.29; N, 7.91; Cu, 9.00
λ_{max}: 287,337 nm.
ESI-MS [MeOH, *m/z*]: 702.0 [M^+]

P. [Cu(MFL)(L8)H_2O] **(C8)**

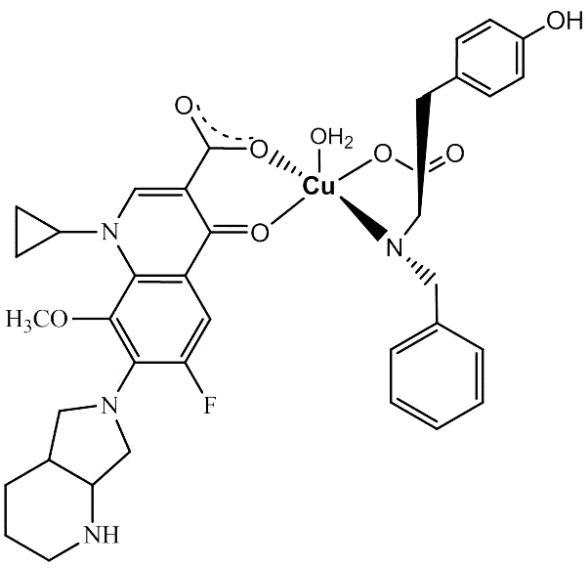

Yield: 71%
Molecular weight: 752.23 g/mol
Molecular formula: $C_{37}H_{42}CuFN_4O_8$
Calc. (%): C, 58.99; H, 5.62; N, 7.44; Cu, 8.44
Found (%):C, 59.01; H, 5.59; N, 7.44; Cu, 8.44
λ_{max}: 288, 339 nm.
ESI-MS [MeOH, *m/z*]: 753.09 [M+1]

5.4 Results and discussions

5.4.1 Synthesis and general properties

Ternary copper(II) complexes [Cu(**L1-L4**)(MFL)(H_2O)](**C1-C4**) having ferrocence conjugated mannich base and Moxifloxacin (MFL) as one of the ligand were prepared in good yield (~80%) from reaction of ferrocenyl mannich bases (**L1-L4**) with copper(II) acetate monohydrate and MFL in methanol (Scheme 5.3). To explore the effect of the ferrocenyl moiety on the overall DNA cleavage activity and cytotoxicity of C1-C4, complexes [Cu(**L5-L8**)(MFL)(H_2O)](**C5-C8**) were prepared, with MFL and mannich bases derived from benzaldehyde and L-amino acids (**L5-L8**).

The complexes were characterized by various spectroscopic and analytical methods. The ESI-MS spectra of the ligands **L1–L8** and their complexes **C1–C8** showed molecular ion peaks at m/z values equivalent to their molecular weights. The m/z values of all the complexes are in well agreement with the proposed composition (Section 5.3). Furthermore the composition and purity of the complexes have been confirmed by their C, H, N elemental analysis (Section 005.3).

The FTIR spectra of the complexes **C1–C8** displayed characteristic strong stretching bands at 1518–1582 cm^{-1} and weaker bands at 1490–1514 cm^{-1} due to asymmetric and symmetric carboxylate (COO^-) stretch respectively, which were are found as strong bands in the fingerprint region at 1580–1612 cm^{-1} in the spectra of free ligands **L1–L8**. Moreover the distinct broad bands in the range 3414-3480 cm^{-1} owing to the O-H stretching of free carboxylic acid group found in the ligands was completely lost in the IR spectra of the complexes indicating complexation of the ligands with the metal ion via the carboxylate oxygen (Fig 5.1(a) and Fig 5.1(b)). Furthermore the medium secondary amine N-H stretching bands found in the spectra of the free ligands **L1– L8** in the region of 2921–

2963 cm^{-1} shifted to 2927–2951 cm^{-1} in **C1–C8** indicating complexation of the ligands via the nitrogen of secondary amine (mannich base).

Similarly the shifts in the pyridone carbonyl $\nu(CO)_{MFL}$ and carboxylate $\nu(COO)_{MFL}$ stretching frequencies of moxifloxacin in complexes indicated the binding of these groups with the metal ion. All the important stretching values have been tabulated in Table 5.1.

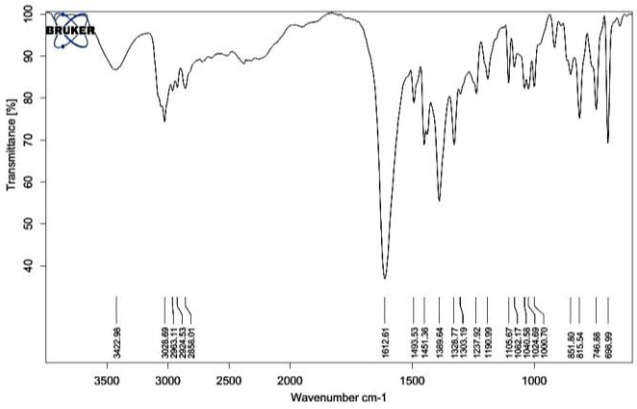

Fig 5.1(a): IR spectra of **L2**

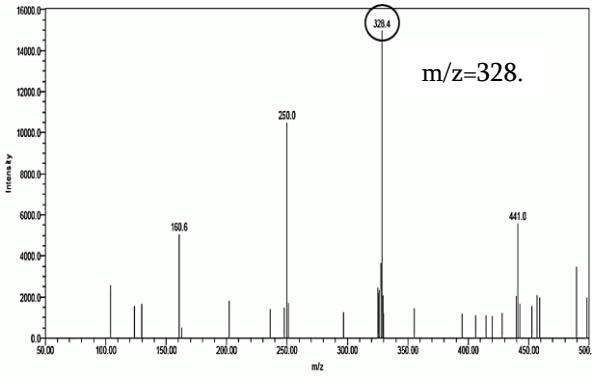

Fig 5.2(a): ESI-MS spectra of **L2**

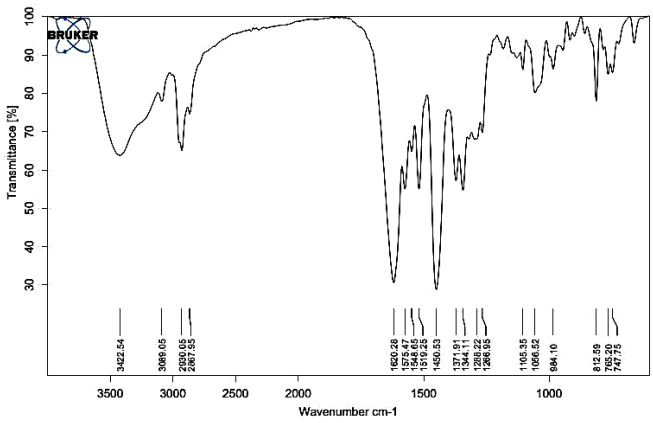

Fig 5.1(b): IR spectra of **C2**

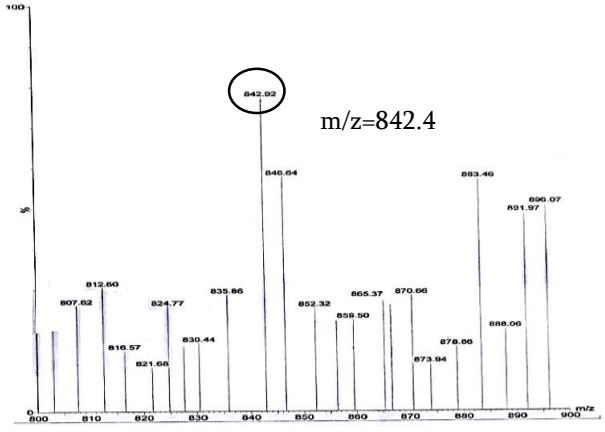

Fig 5.2(b): ESI-MS spectra of **C2**

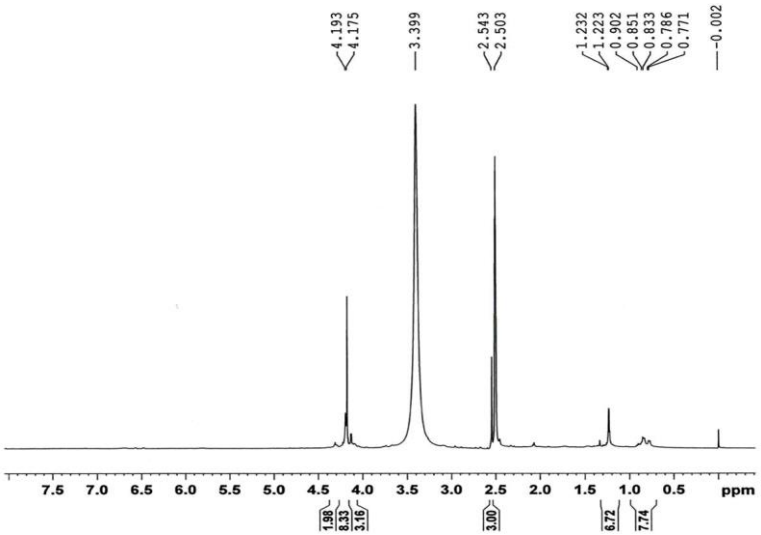

Fig 5.3: ^{1}H NMR spectra of **L3.**

Table 5.1: Characteristic IR bands (4000–400 cm^{-1}) of **L1-L8** and **C1-C8**.

Compounds	IR stretching values (cm^{-1})							
	υ_{N-H}	Fc-AA/BzAA Free COOH stretch		$\upsilon_{(COO)}$ assym	$\upsilon_{(COO)}$ sym	MFL	$\upsilon_{(COO)}$ assym	$\upsilon_{(COO)}$ sym
		υ_{O-H}	$\upsilon_{C=O}$			$\upsilon_{(C=O)p}$		
MFL	-	-	-	-	-	1708	1624 (Free COOH)	
L1	2925	3444	1597	-	-	-	-	-
L2	2963	3422	1612	-	-	-	-	-
L3	2956	3462	1604	-	-	-	-	-
L4	2921	3420	1580	-	-	-	-	-
L5	2960	3426	1595	-	-	-	-	-
L6	2944	3426	1562	-	-	-	-	-
L7	2952	3480	1602	-	-	-	-	-
L8	2951	3414	1582	-	-	-	-	-
C1	2920	-	-	1518	1481	1621	1448	1347
C2	2928	-	-	1519	1497	1621	1451	1345
C3	2930	-	-	1519	1481	1620	1450	1344
C4	2926	-	-	1517	1496	1621	1448	1346
C5	2927	-	-	1519	1490	1620	1451	1345
C6	2926	-	-	1519	1495	1619	1452	1343
C7	2927	-	-	1582	1514	1619	1452	1345
C8	2930	-	-	1574	1508	1620	1450	1345

The ^{1}H NMR spectra of ligands **L1-L4** show 9 proton multiplet in the δ range of 4–5 ppm that can be ascribed to the ferrocenyl ring protons. The singlet signals at δ= 1–2 pertains to the N—H and COO—H proton of the amino acids. The spectrum of L3, apart from the above mentioned signals, also shows a 6 proton singlet at δ=1.2 ppm owing to two methyl groups—CH $(CH3)_2$ of leucine (Fig 5.3). Whereas the spectrum of **L1** shows 5 proton multiplet in the δ range of 7–8 ppm ascribable to the aromatic protons of the tryptophan and a one proton singlet at δ = 11 ppm attributed to the indoyl N—H.

The electronic absorption spectra of the ligands **L1-L8** and complexes **C1-C8** in DMSO solution were recorded in the region 200-900nm. The electronic spectra of free ligands **L1-L4** and **L5-L8** displayed intense absorption bands in the UV region ascribed to π-π* intra ligand transition of the cyclopentadienyl rings of ferrocene and benzene ring respectively, which were observed to in the spectra of the complexes **C1-C8** (Table 5.2). The intra ligand transition bands of complexes **C1-C8** were observed at longer wavelength region at 289-290 nm (Fig. 5.3) due to coordination with Cu(II). In addition, all the complexes showed peaks in the region 336-340 nm corresponding to π-π* transitions of MFL ligand (Fig. 5.3). Absorption bands at 402-417nm were ascribed to MLCT transitions of coordinated MFL ligand. Broad absorptions observed in the range 619-637 nm (ε =2.2 M^{-1} cm^{-1}) were attributed to d–d transitions for Cu (II) in square pyramidal geometry [34].

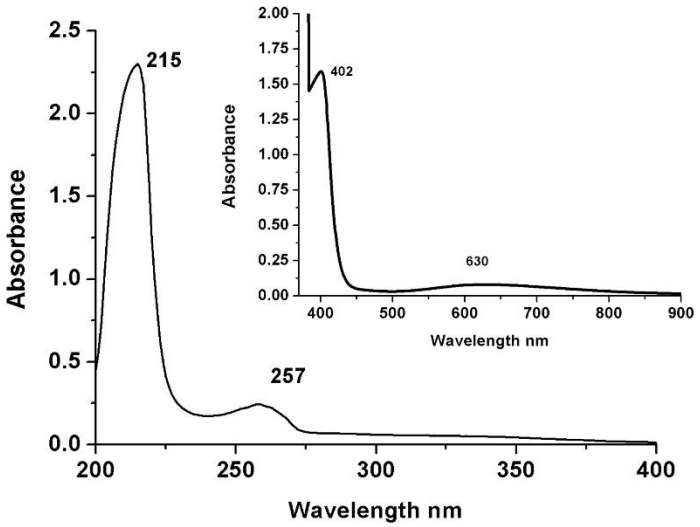

Fig 5.3: Electronic spectra of **L2** in dmso. Inset shows the visible spectra of the complex **C2**.

Table 5.2: Electronic spectral data of ligands (**L1-L8**) and complexes (**C1-C8).**

Compound	Intraligand charge transfer transitions π-π^*	CT nm	d-d Transition nm
L1	218, 265(sh), 329	-	-
L2	216, 251(sh), 321	-	-
L3	216, 249(sh), 320	-	-
L4	208, 225(sh), 283	-	-
L5	215, 260	-	-
L6	215, 257	-	-
L7	213, 259	-	-
L8	220, 276	-	-
MFL	288, 330	-	-
C1	205, 289, 339	406	628
C2	206, 290, 337	417	631
C3	205, 290, 338	402	619
C4	204, 290, 336	409	627
C5	216, 290, 338	402	629
C6	205, 289, 337	402	630
C7	206, 289, 339	402	637
C8	204, 290, 338	402	632

The ESR spectra of **C2** and **C7** were recorded in DMSO at 10 K using 90 KHz field modulation and the *g* factors were quoted relative to the standard marker TCNE (g = 2.00277). The complexes exhibited axial EPR spectra with good hyperfine splitting (Fig. 5.5) and the corresponding $g_{\|}$, $g_{\perp}$ and $A_{\|}$ values are tabulated in Table 3. **C2** and **C7** exhibit axial EPR spectra with g_{II} = 2.23-2.32, $g_{\perp}$=2.0-2.1 and A_{II} values ranging from 140-146×10^{-4} respectively. The $g_{II} > g_{\perp} > 2.0023$ values indicated that the unpaired electron of Cu (II) most likely resides in d_{x2-y2} orbital having $^2B_{1g}$ as ground state and the complexes have distorted square pyramidal geometry. The axial symmetry parameter (G>4.2) indicated that there are no spin exchange interactions between the copper centres (G>4).

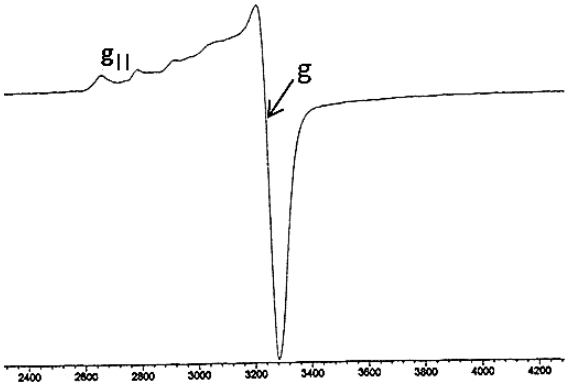

Fig 5.5: ESR Spectra of **C2** in DMSO.
EPR conditions: Temperature, 10K; microwave power, 5.0 mW; Modulation amplitude, 1G; microwave frequency, 9.1GHz.

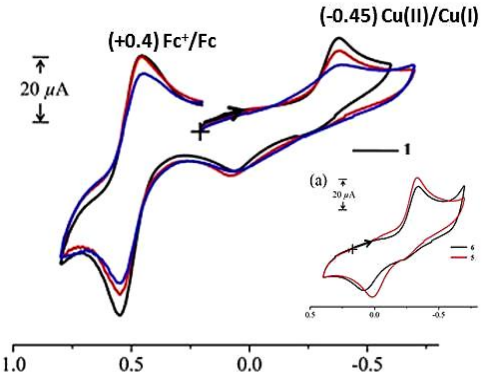

Fig 5.6: Cyclic voltammogram of **C2** in dmso - 0.1 M TEAP at a scan speed of 50 mV s^{-1}

Complexes **C1-C8** were redox active and displayed a quasi-reversible cyclic voltammetric response near 500 mV vs SCE in dmso assignable to the Fc^{+}-Fc couple, where Fc is the ferrocenyl moiety (Table 5.3, Fig. 5.6). There was a significant positive shift of ~50 mV in the Fe(III)/Fe(II) potential in these complexes compared to that of only ferrocene (430 mV vs SCE). The copper(II) complexes also showed a quasi-reversible cyclic voltammetric response in the range 380-470 mV assigned to the Cu(II)-Cu(I) redox couple.

Table 5.3: ESR and cyclic voltammetric data of **C1-C8**.

Compounds	C1	C2	C3	C4	C5	C6	C7	C8
$g_{\|\|}$	-	2.23	-	-	-	-	2.32	-
$g^{\perp}$	-	2.09	-	-	-	-	2.12	-
$A_{\|\|}$	-	140×10^{-4}	-	-	-	-	146×10^{-4}	-
$A^{\perp}$	-	48×10^{-4}	-	-	-	-	50×10^{-4}	-
Fc^{+}/Fc	480	470	485	480	475	481	485	480
Cu^{2+}/Cu^{1+}	-450	-470	-440	-420	-380	-410	-400	-385
Cu^{1+}/Cu^{2+}	290	290	275	250	250	255	250	245
ΔEp (mV)	-160	-180	-165	-170	-130	-155	-150	-140

Thermal stability of all the complexes **C1-C8** were studied by thermogravimetric analysis in the temperature range 50–850°C in N_2 atmosphere. The correlations between the different decomposition steps of the complexes with the corresponding weight losses are discussed in terms of the proposed formula of the complexes. The thermal behaviour studies of all the complexes were found to be similar.

The TGA profiles over the temperature range 30–250 °C are usually due to loss of moisture, water of hydration and coordinated water. The first decomposition step in the range 200–250°C was due to loss of coordinated water. Above 250 °C, complexes decompose in a gradual manner upto 700 °C, due to thermal degradation of the organic moiety (mannich bases and MFL, Fig. 5.7(a) leaving CuO as residue (Fig. 5.7(b)). From the above thermogravimetric analyses, the overall weight losses for the complexes agree well with the proposed formula obtained by elemental analyses, IR, mass and ESR measurements.

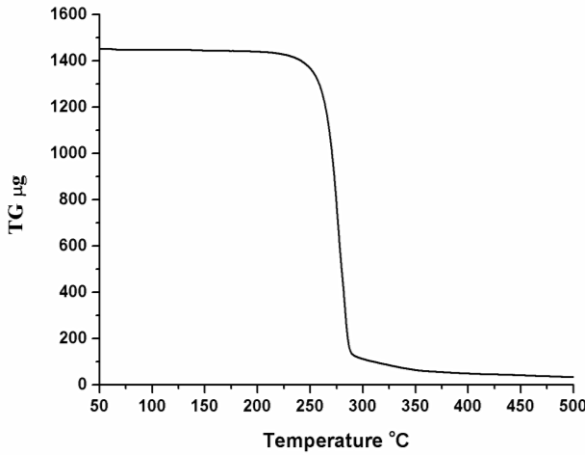

Fig 5.7 (a): Thermal degradation curve of **L2** at heating rate of 10 °C per minute u nder N_2 atmosphere.

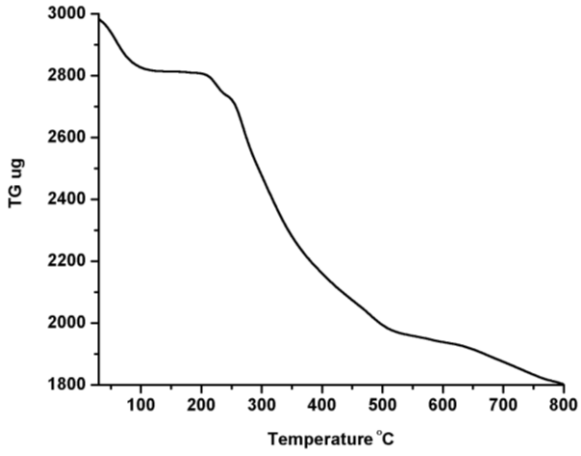

Fig 5.7 (b): Thermal degradation curve of **C2** at heating rate of 10 °C per minute under N_2 atmosphere.

5.4.2. DNA binding studies

5.4.2.1 UV-Visible absorption titration

The presence of ground state interactions between the biological macromolecule DNA and compounds under study have been detected using absorption spectroscopy. DNA can provide three distinctive binding sites (groove binding outside of DNA helix, along major or minor groove, electrostatic binding to phosphate group and intercalation), a behaviour important for the biological role of antibiotic and anticancer drugs in vivo [34]. The binding efficiency of metal complex to DNA can be effectively investigated employing electronic spectroscopy since the observed changes in the spectra may give evidence of the existing interaction mode [34, 35]. Any interaction between the compounds (**LI–L8 and C1–C8**) and DNA is expected to perturb the ligand centred transitions of the compounds.

Binding with DNA via non-intercalative binding modes, such as electrostatic forces, van der Waals interactions, hydrogen bonds and hydrophobic interactions generally results in increase in absorption intensity (hyperchromism) and blue shift of the absorption bands upon increasing the concentration of CT-DNA owing to the degradation of the DNA double helix structure. A blue shift may also be attributed to improper coupling of π^* orbital of the ligand and π orbital of the base pairs. This unstacking of base pairs (distortion in π orbital of base pairs and π^* orbital of ligand) causes slight blue shift (hypsochromic shift). Similarly reduction of face to face base stacking (exposed electrons) induces enhancement of absorption intensity (hyperchromism). On the other hand intercalation generally results in hypochromism and a red shift (bathochromism) of the absorption band due to a strong stacking interaction between an aromatic moiety of the ligand and the base pairs of the DNA. A red shift can be directly linked with π^* orbital of intercalated compounds couple with the π orbital of DNA base pairs, thus decreasing π-π^* transition energy. On the other hand the coupling π orbital is partially filled by

electrons thus decreasing transition probabilities and concomitantly resulting in hypochromism [36].

The UV spectra of ligands **L1–L8** (10^{-6}M) and complexes **C1-C8** (10^{-6} M), have been recorded in absence and presence of varying CT-DNA concentration (1–50 x 10^{-3} M) within. The absorption bands of the ligands **L1–L8** centred at 208-220 nm showed significant hypochromism and a slight red shift. The observed hypochromic shift may suggest tight binding to CT-DNA via intercalation and red shift symbolises stabilisation of DNA duplex. In case of complexes **C1–C8**, bands centred around 289–290 nm (band I) and 337-339 (band II), showed significant hyperchromism with red shift (Fig.5.8), speculative of primarily groove binding nature of the compounds. It should be noted that the exact mode of interaction with DNA cannot be concluded only by UV spectroscopic studies and more techniques should be combined in order to come to a safe conclusion. The existing results from the UV titration experiments suggested that all compounds bind to CT DNA [37]; in the cases where an hyperchromic effect exists, a first evidence of binding to CT DNA probably by groove binding may be suggested, while the existence of a red-shift is a hint of a stabilization of the DNA duplex provoked by such interaction [38].

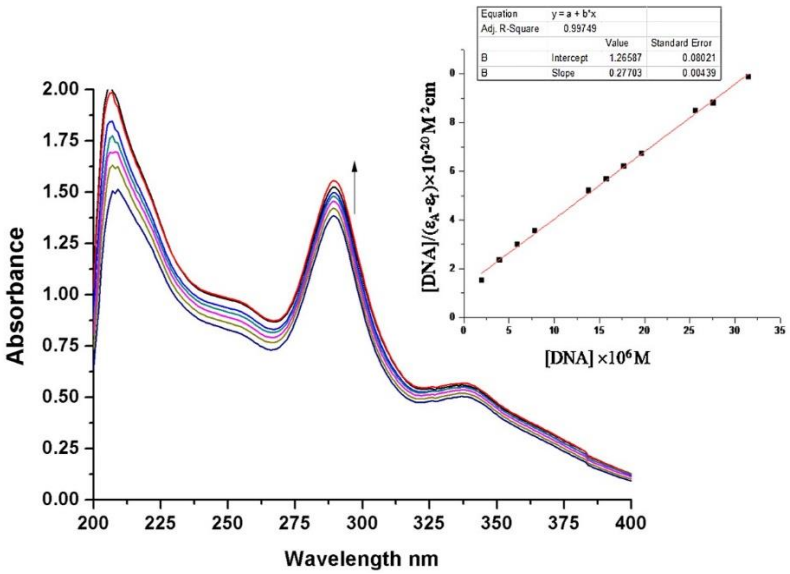

Fig 5.8: Absorption spectraof **C1** showing the increase in absorption intensity on gradual addition of CT-DNA in 5 mM TrisHCl buffer(pH,7.2) at 25°C. Inset shows the plot of [DNA]/(ε_A-ε_f) vs [DNA].

The magnitude of binding strength to CT-DNA can be determined through the calculation of binding constant K_b, which is obtained by monitoring the changes in the absorbance of the compounds with increasing concentrations of CT-DNA. K_b is given by the ratio of slope to the y intercept in plots [DNA]/(εa– εf) versus [DNA]. where $\varepsilon_a = A_{obsd}$/ [compound], ε_f is the extinction coefficient for the unbound compound (**L1-C8**) and ϵ_b is the extinction coefficient for the compound in the fully bound form. The binding constant K_b values (Table 5.3) for the ligands were in the range of $1.3x10^4$–$6.7x10^4$ M^{-1} indicative of strong binding of the ligands with DNA, **L1** showing the highest binding constant. The K_b values

In general, complexes **C1–C4** exhibit olds higher binding efficacy compared to stronger binding interactions(10^6 M^{-1}) than complexes **C5–C8** (10^5 M^{-1}) due to groove binding of the ferrocenyl moiety. Complex **C1** with a trytophan substituted ferrocenyl moiety bound to the Cu (II) center shows the highest binding constant value due to additional hydrogen bonding interaction between —NH group of tryptophan and DNA nucleobases . **C4** with a tyrosine substituted ferrocenyl moiety shows similar binding constant as C1 which also may be due to additional hydrogen bonding interactions between —OH group of tyrosine and DNA nucleobases which are accessible both in major groove. nucleobases which are accessible both in major and minor groove.

Table 5.3: DNA binding constants (K_b) of ligands **(L1-L8)** and complexes (**C1-C8)**

Compound	% Hypo/Hyper chromism	K_b
L1	18%	6.7×10^4
L2	12%	1.4×10^4
L3	19%	1.3×10^4
L4	20%	5.8×10^4
L5	15%	2.0×10^4
L6	20%	1.5×10^4
L7	17%	4.0×10^4
L8	19%	3.4×10^4
C1	36%	7.0×10^6
C2	25%	2.3×10^6
C3	30%	4.2×10^6
C4	34%	6.4×10^6
C5	39%	6.0×10^5
C6	34%	2.5×10^5
C7	30%	3.4×10^5
C8	36%	5.2×10^5

5.4.2.2 Fluorescence quenching Studies

To further examine the mode of binding of the compounds with DNA, via intercalation or groove binding, a competitive binding study with two dyes: EB and DAPI have been carried out using steady state fluorescence spectroscopy

5.4.2.2.1 Competitive DNA binding studies with EB

Ethidium bromide (=3,8-diamino-5-ethyl-6-phenyl-phenanthridinium bromide) is a phenanthridine fluorescence dye and is a typical indicator of intercalation, forming soluble complexes with nucleic acids and emitting intense fluorescence in the presence of CT DNA due to the intercalation of the planar phenanthridinium ring between adjacent base pairs on the double helix [39]. Addition of a second molecule, which may replace and bind to DNA via intercalation than EB results in a decrease of the DNA-induced EB emission [40]. The emission spectra of DNA–EB (λ_{ex}= 546 nm, λ_{em}= 610) in the absence and presence of increasing amounts of ligands and complexes have been recorded. Addition of the ligands **L1–L8** or the complexes **C1–C8** did not have any kind of effect on the emission intensity or nature of the emission of DNA–EB complex, indicating that intercalation may not be the binding mode for compounds.

Competitive binding studies with DAPI

DAPI (4,6-diamidino-2-phenylindole) is a classical minor groove binder to DNA and binds specifically to GC regions by intercalation; however, the minor binding to AT regions is two orders of magnitude stronger than the intercalative binding mode. The fluorescence of DAPI increases approximately 30 times when excess (base pairs) of DNA is added to the solution of the dye [41,42]. The fluorescence spectra of a mixture of DNA–DAPI solution with increasing concentration of **C1–C8** (0-100μM) have been recorded . The addition of aliquots of the complexes caused an initial fluorescence enhancement (Fig. 5.10, red lines) which on further addition showed subsequent quenching of the DNA–DAPI fluorescence (Fig. 5.10,

blue lines). The initial fluorescence enhancement can be attributed to partial overlap of the electronic states of the quencher molecules (**C1–C8**) and DNA–DAPI complex leading to partial stabilization of the ground state complex and an increase in the value of the Franck–Condon factor. The fluorescence intensity is proportional to the overlap of vibrational wave functions and consequently to the Franck–Condon factor.

A quencher molecule when approaches a DNA–DAPI complex, forms an intermediate complex, which is temporarily more stable than the original DNA– DAPI complex. This shifts the ground electronic state to left and down, and as a result the overlap between the vibrational functions in the excited and ground electronic states increases due to the Frank–Condon principle (greater the overlap between the vibrational functions of excited and ground states of the complex, greater is the Franck–Condon factor), leading to the increase in fluorescence signal. Further addition of the quencher leads to the complete displacement of DAPI from the DNA helix and fluorescence depletion [43]. This phenomenon has been explained schematically in Fig. 5.11. The quenching of the DNA–DAPI fluorescence is conclusive of the fact

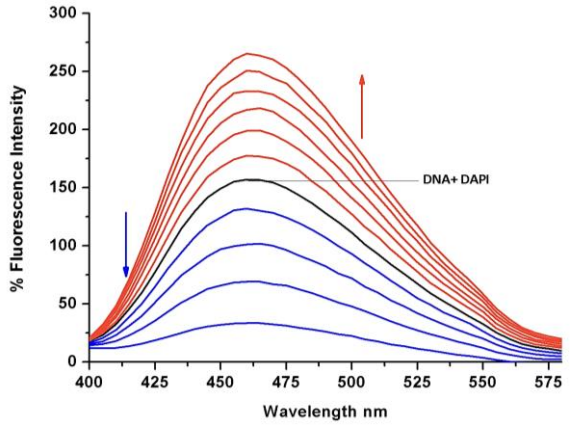

Fig 5.10: Emission titration of DNA-Dapi complex with increasing concentration of **C1**.
Red lines = changes in 1st phase (increasing intensity); blue lines= changes in 2nd phase (decreasing intensity).

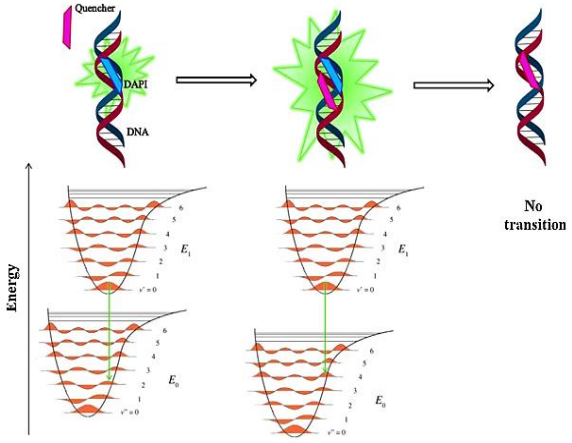

Fig 5.11: Schematic presentation of DAPI displacement from DNA helix by quencher molecule followed by fluorescence quenching and corresponding energy diagrams.

that complexes **C1–C8** replace DAPI from the minor grooves of DNA and themselves get bound indicating their preference for groove binding.

5.4.2.3 Viscosity Measurements

In order to further confirm the modes of binding of **C1–C8** to CT-DNA, viscosity measurements of DNA solutions were carried out in presence and absence of these complexes. The viscosity of DNA is sensitive to length changes and is regarded as the least ambiguous and the most critical clues of a DNA binding mode in solution [44].

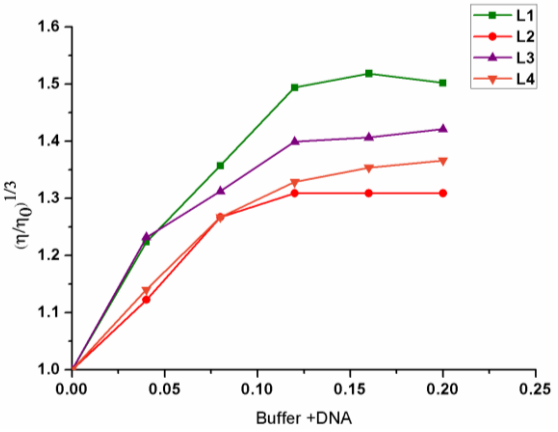

Fig 5.12 (a): Effect of increasing amounts of the complexes **L1–L4** on the relative viscosity of CT-DNA (200 mM) in Tris–HCl buffer at 25°C. [Complex]/[DNA] = 0, 0.04, 0.08, 0.12, 0.16, 0.20 .

In general, intercalating agents are expected to elongate the double helix to accommodate the ligands in between the base pairs, leading to an increase in the viscosity of DNA. In contrast, a complex that binds exclusively in the DNA grooves typically causes less pronounced (positive or negative) or no changes in DNA solution viscosity [45]. The effects of the complexes **C1–C8** , the classical intercalator EB and the groove binder dapi on the viscosities of CT-DNA solution are shown in Fig.5.12(b).

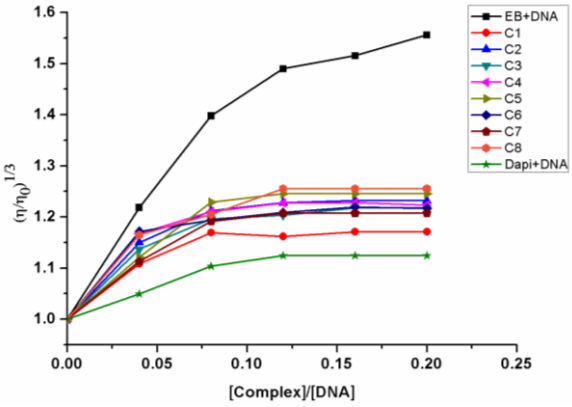

Fig 5.12 (b): Effect of increasing amounts of the complexes **C1–C8**, Dapi and ethidium-bromide (EB) on the relative viscosity of CT-DNA(200 mM) in Tris–HCl buffer at 25 °C. [Complex]/[DNA] = 0, 0.04, 0.08, 0.12, 0.16, 0.20.

For Ligands **L1-L8** with increasing [ligand]/[DNA] concentration ratios, the relative viscosity of CT-DNA increased gradually (Fig 5.12(a)) indicative of

characteristic intercalative mode of binding which was in accordance with previous findings. In contrast with increasing [complex]/[DNA] concentration ratios for complexes **C1–C8** no significant change in the relative viscosity of CT-DNA solution was observed which ruled out intercalative binding mode of complexes and was consistent with the DNA groove binding.

5.4.2.4 Nuclease activity

In order to explore the DNA cleavage activity of present complexes, pBR322 DNA (30μM) was incubated with **C1-C8** (10μM) in 5 mM Tris–HCl/50 mM NaCl buffer solution (pH 7.2). The DNA cleavage activity was assessed by the conversion of supercoiled form of DNA (Form I, SC form) to linear open (Form II, OC) or nicked circular DNA(Form III, NC form). It was found that all the complexes (**C1**-**C8**) exhibited DNA cleavage by the conversion of SC Form (I) into OC Form (II) (Fig. 5.13), which indicated that the complexes are involved in the cleavage through single strand breaking. The control experiments with the **L1-L8** or $CuCl_2{\cdot}6H_2O$ or DNA alone did not reveal any significant cleavage.

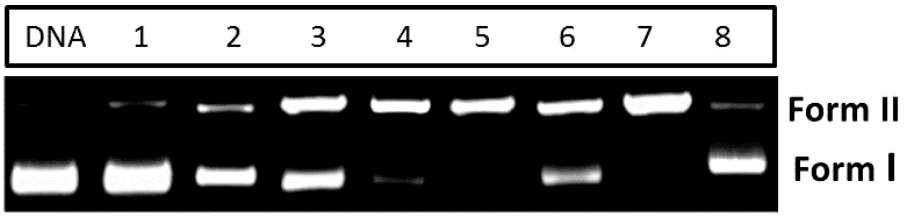

Fig 5.13: Photogenic view of interaction of pBR322 DNA (30 μg/mL) with 10 μM complexes incubated for 2hours at 37 °C: Lane 1, **DNA**; Lane 2, DNA+**C1**; Lane 3, DNA + **C2**; Lane 4, DNA + **C3**; Lane 5, DNA + **C4**; Lane 6, DNA + **C5**; Lane 7, DNA +**C6**; Lane 8, DNA +**C8**.

5.4.3 Cytotoxicity studies

5.4.3.1 MTT assay

3-(4,5-Dimethylthiazol-2-yl)-2,5-diphenyltetrazolium bromide (MTT) assay was done to test the ability of compounds to inhibit cell growth and induce death in A549 cells(human lung carcinoma). A549 cells when treated with the compounds at varying concentrations (15–250μg/ml) for 12 h, inhibited their growth significantly in a dose and time dependent manner and recorded 50–85% higher cytotoxicity compared to the ligands. The IC_{50} values shown in Fig. 5.14 indicated the order of cytotoxicity as C7<C6<C8<C5<C3<C2<C4<C1. The results revealed enhancement in the antiproliferative activity of the parent fluoroquinolone ligand (MFL) upon metal (Cu^{2+}) conjugation giving credence to the hypothesis that biological activity of fluoroquinolones may partly be related to their metal chelating ability. Cell viability assay using control compounds showed that the ligands and the metal salt alone were nontoxic to the cancer cells. Amongst the compounds examined presently, the **C1** seemed to be the most potent molecule.

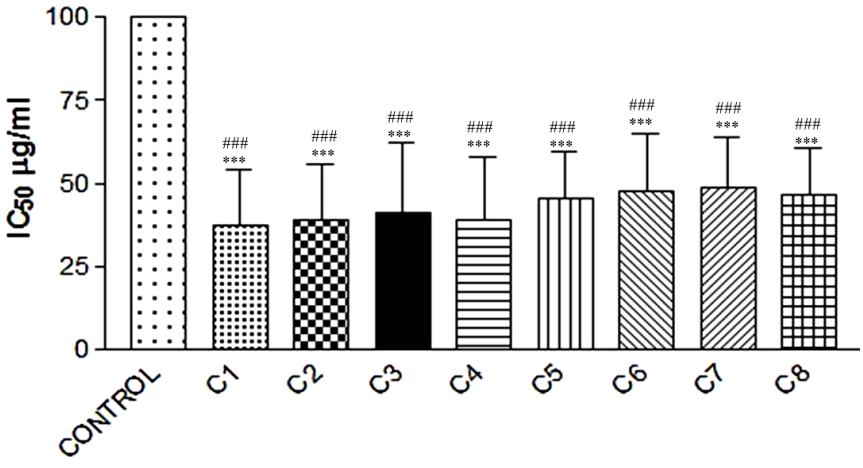

Fig 5.14: Data expressed as mean ±S.E.M. for n=3. Where, ***p<0.001 compared to Ligands (**L1-L8**) and ###p<0.001 compared to MFL. 50% inhibition concentration (IC_{50} μg/ml) for Complexes **C1–C8**.

5.4.3.2 Cellular uptake study

The localization of **C1-C8** inside A549 cells, were studied by confocal microscopy. A549 cells were cultured on coverslips (corning22x22 mm), incubated for 24 h until they reached 70% confluency. These were then serum starved overnight, followed by incubation with **C1-C8** (IC_{50}), for 6h at 37°C. Confocal microscopy imaging was carried out by staining with PI (nuclear stain) to identify localization of the complexes and any nuclear disintegration. The cell-membrane is the structure that protects living cells from the surrounding environment, allowing the movement of compounds generally with small molecular size across this barrier into the cell. As the complexes were stable in aqueous solution and their luminescence intensity increased upon binding with DNA, therefore their cellular uptake properties of present complexes could be studied using confocal microscopy [45]. After treatment for 6 h, cells were observed under confocal microscope. On treatment with **C1**, bright blue fluorescence in the cytoplasm of the cells was observed (Fig. 5.15(A)), indicating the uptake of **C1** by cells. Fluorescence intensity was found to increase with time indicating increased internalization of the complexes. Similar results were observed for **C2-C8**, which indicated that complexes **C1-C8** can enter and accumulate in cytosol of cell.

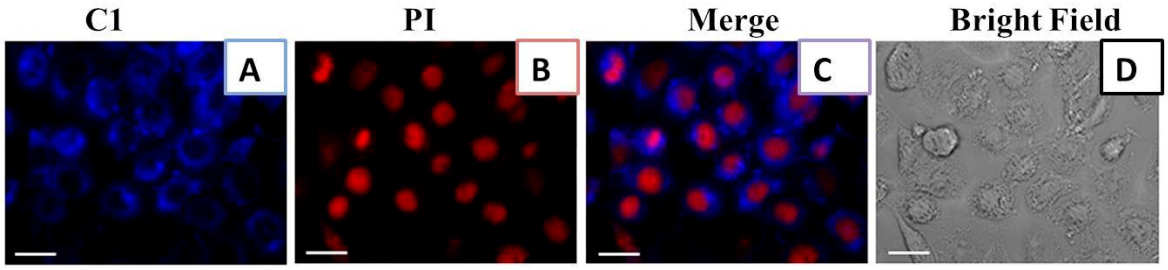

Fig 5.15: Confocal microscopic images of A549 cells treated with C1 and PI (A) blue emission of **C1** (B) nucleus stained with PI (C) Merged image of A and B (D) Bright field image of A549 cells treated with **C1** for 6 hr at 37°C.

5.4.3.3 Induction of Apoptosis

Apoptosis induced by compounds is one of the considerations in drug development. The apoptotic cells usually show characteristic apoptotic features such as nuclear shrinkage and chromatin condensation. Apoptosis assay was carried out with staining methods using acridine orange (AO) and ethidium bromide (EB) to assess the changes in nuclear morphology. Apoptotic and necrotic cells can be distinguished from one another using fluorescence microscopy. In the absence of **C1**, the A549 cells were stained bright green (Fig. 5.16(A), control) by AO. After treatment of A549 cells with **C1** for a period of 12 h, revealed presence of apoptotic cells containing apoptotic bodies stained by acridine orange as well as ethidium bromide (Fig. 5.16(A)). Similar results were observed for all the complexes.

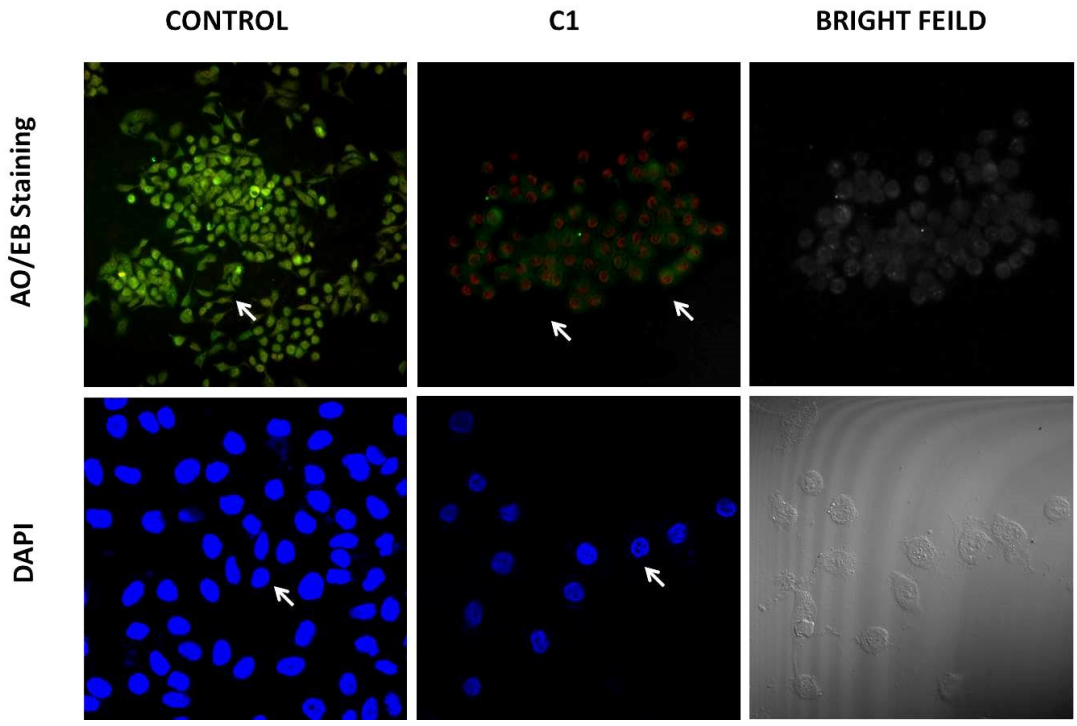

Fig 5.16: confocal images of A549 cells treated with **C1** for 12 hr at 37°C in 5% CO_2. A) Staining with Acridine orange/ ethidium bromide. B) Staining with DAPI.

To further asses the nuclear features and to gain insight into the pathway of cell death, we carried out DAPI staining of A549 cells after incubation with **C1-C8** for 12 h (Fig. 5.16(B)). The control cells exhibit light and evenly stained contours of the nuclei in contrast to the cells treated with **C1** that show typical characteristics of cells undergoing apoptosis (Fig. 5.16(B)). The treated cells are seen to possess fragmented or highly condensed nuclei while the bright field images provide evidence for cell shrinkage and membrane blebbing attributed to the typical features of apoptotic cells (Fig. 5.16). Necrotic nuclei are not observed with DAPI staining. The DAPI staining indicates apoptotic mode of cell death induced by **C1**. Similar results were observed with all the other complexes.

5.4.3.4 Cell cycle arrest by flow cytometry

The effect of **C1-C8** on the cell cycle of A 549 cells was studied by flow cytometry in propidium iodide (PI) stained cells after treatment with complexes for 12 h. The representative DNA distribution histograms of control and A549 cells in the presence of **C1** are shown in Fig. 5.17.

Cells go through the cell cycle in several well-controlled phases [46]. The entry into each phase of the cell cycle is carefully regulated by different checkpoints. One of the major focuses of drug discovery is to develop agents that target the cell cycle checkpoints that are responsible for the control of cell cycle phase progression. Cell cycle analysis is used to detect and measure apoptosis, a form of programmed cell death, by analysing cells with less DNA content ("sub-G_1 cells")[47]. Such cells are usually the result of apoptotic DNA fragmentation. Apoptotic cells often have fractional DNA content due to the fact that the fragmented (low MW) DNA undergoes extraction during the staining procedure. Some cells also lose DNA (chromatin) by shedding apoptotic bodies. Thus, only a fraction of the DNA remains within apoptotic cells. Therefore, nuclei of apoptotic cells contain less DNA than nuclei of healthy G_0/G_1 cells, resulting in a sub-G_0/G_1 peak in the fluorescence histogram that can be used to determine the relative amount of apoptotic cells in a

sample.

Flow cytometry was used to probe the mode of cell death and cell cycle arrest induced by complexes (**C1-C8**), and it was found that after 12 h of treatment with **C1** the population of G0/G1, S, G2/M cells decreased without significantly affecting the overall cell count (Fig. 5.17a). Moreover, on treatment with complexes the percentage of cells is increased in the Sub G0/G1 phase (Fig. 5.17 (a) & (b)) reflecting a significant inhibition of cell cycle progression. Thus, the overall effect of **C1** treatment appears to involve the prevention of cell division followed by cell death with a profile indicative of programmed cell death (apoptosis). Similar results were obtained with complexes **C2-C8** (Fig. 5.17(b)).

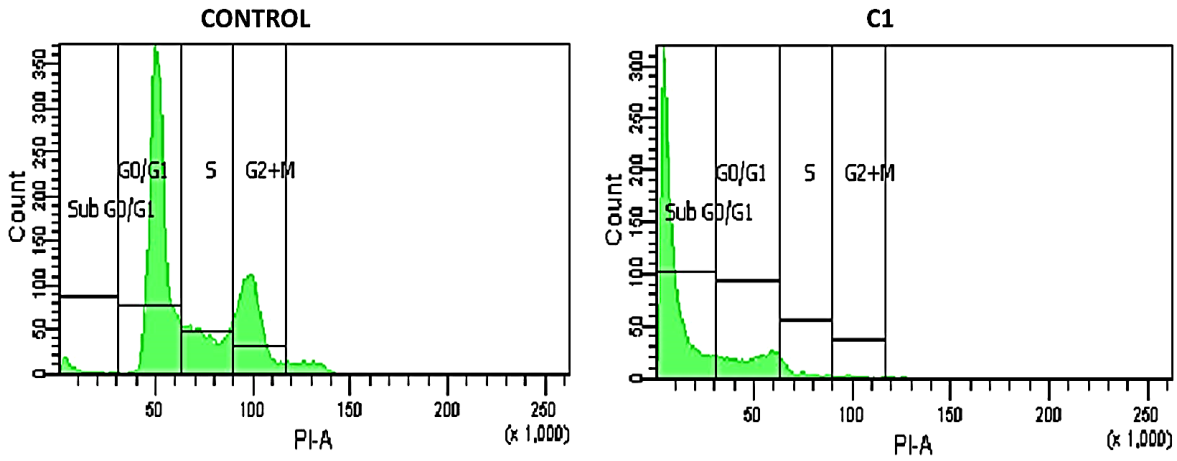

Fig 17 (a): Effects of **C1** on A549 tumor cells after 12 h, distribution among cell cycle phases.

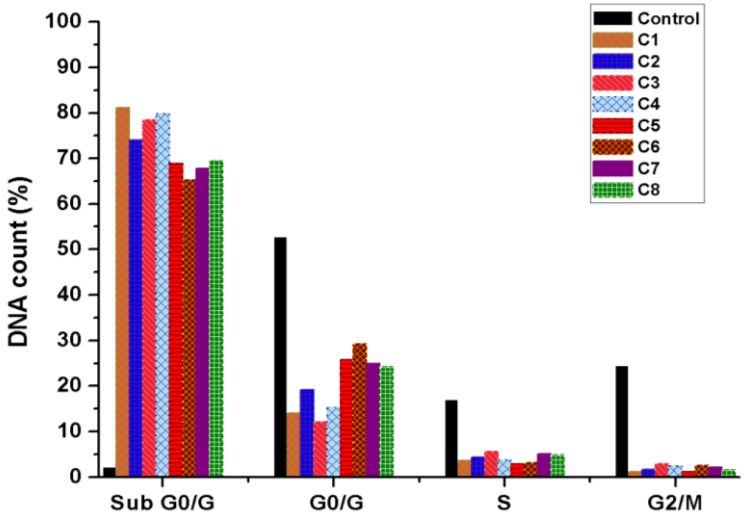

Fig 17 (b): Cell cycle distribution on exposure of A549cells to complexes **C1-C8** (IC_{50}).

An apoptosis study using flow cytometer can be used to distinguish different cell types such as viable cells, early apoptotic cells, and late apoptotic cells [48]. The measurement of annexin V binding to the cell surface as an indicator for apoptosis was performed along with a dye exclusion test to establish the integrity of the cell membrane. Annexin V, a calcium-dependent phospholipid binding protein with high affinity for phosphatidylserine, binds to the phosphatidylserine that has migrated outside the cell membrane in apoptotic cells. Propidium iodide (PI), binds to the nucleus once the cell membrane has broken down, was used as an indicator of membrane structural integrity.

In the early stages of apoptosis, the cell membrane can exposes phosphatidylserine, which binds to annexin . Viable cells did not bind to annexin V or PI ($FITC^{-}P^{-}$; lower-left quadrant), early apoptotic cells bound to annexin V but excluded PI ($FITC^{+}$ PI^{-}; lower-right quadrant), and late apoptotic cells were positive for both annexin V and PI ($FITC^{+}$ PI^{+}; upper-right quadrant). The upper-left quadrant contains dead cells (necrotic cells; $FITC^{-}$ PI^{+}). The results are shown in Fig.5.18 (a) & 5.18 (b). The results indicate that the control contains mostly live cells, with 3.59 % late apoptotic cells (upper-right quadrant). The increasing order of the percentage of late apoptotic cells in A549 cells treated with complexes **C1**–**C8** (IC_{50}) for 12 h is given by: **C2< C7 < C5 < C8 < C4 < C6 < C3 < C1** (**C1**–36.6 %, **C2**–21.3 %, **C3**–33.1 %, **C4**–29.3 %, **C5**-27.4%, **C6**-31.1%, **C7**-22.8% and **C8**-27.6%) (Fig. 5.18(b)). These results indicate that the cytotoxic complexes **C1-C8** induce apoptosis of the A549 cells.

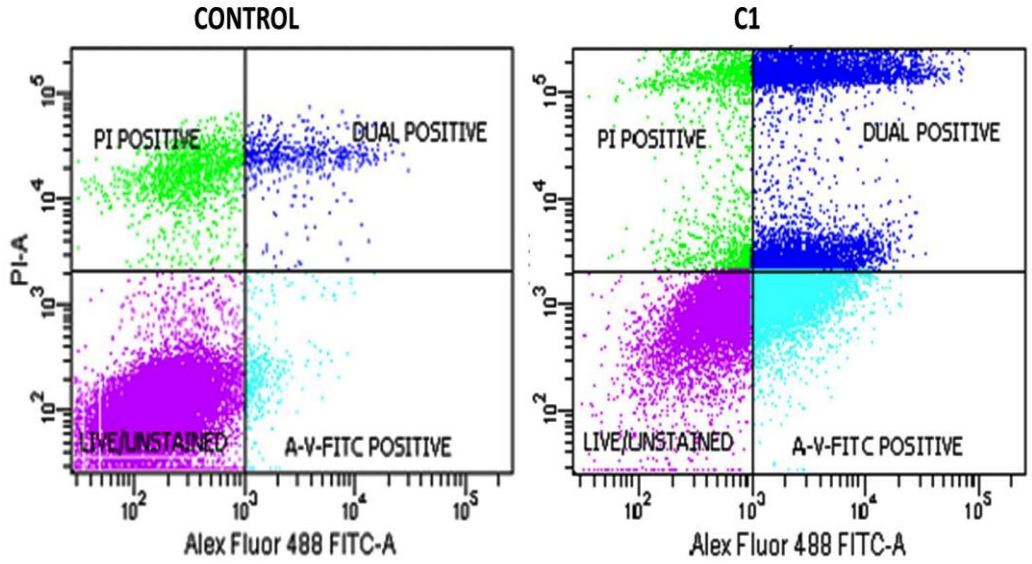

Fig 5.18 (a): Annexin V staining shows induction of apoptosis of A549 cells treated with **C1** for12 h. The percent of apoptotic cells were detected by analysing Annexin V and PI binding with the help of flow cytometry. Viable cells did not bind to Annexin V or PI (lower left quadrant D3), early apoptotic cells bound to Annexin V but excluded PI (lower right quadrant D4), and late apoptotic cells were both annexin V- and PI-positive (upper right quadrant D2), the upper left quadrant D1 contains the nuclear debris or dead cell.

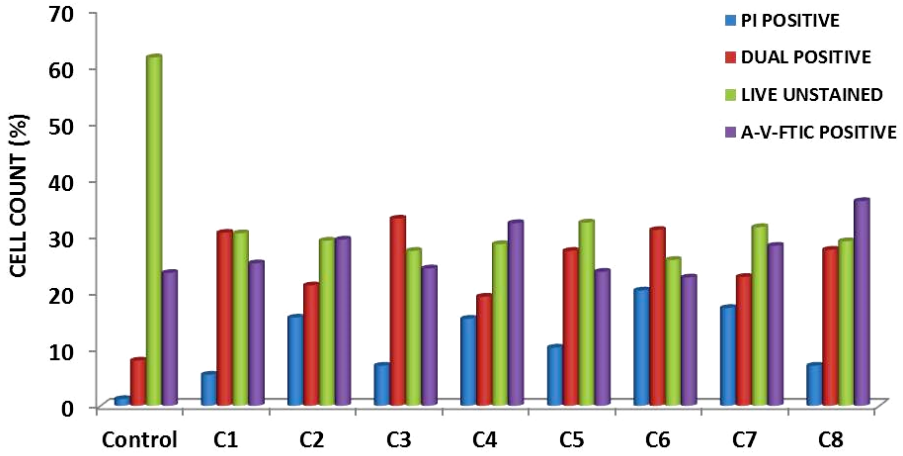

Fig 5.18 (b): Graphical representation of flow-cytometric analysis of apoptosis induced in A549 cells on treatment with C1-C8 for 12 h. Data is represented in the form of percentage of apoptotic population.

5.5 Conclusion

Ferrocene-conjugated L-Amino acid mannich base ternary complexes with copper(II) and moxifloxacin were synthesized and characterized and their potential as cytotoxic agents was studied. Binding of these complexes to CTDNA was been investigated in details by electronic absorption titration, steady state emission, and viscosity studies. The results suggest that ferrocenyl conjugates (**C1-C4**) are efficient groove binders to CT DNA. The redox active complexes with quasi-reversible Fc^{+}/Fc and Cu(II)/Cu(I) couples display significant chemical nuclease activity (pBR322 DNA) in absence of any external agents.

Antiproliferative effects on A549 tumor cells exerted by above complexes are consistent with their intracellular uptake properties. The cellular uptake studies indicated that complexes **C1-C8** enter the cytoplasm and accumulate in the nuclei. Rapid changes in the nuclear morphology with DAPI staining and acridine orange/ethidium bromide dual staining revealed that most of the A549 cells enter early apoptosis within 12 h of treatment. Further all the complexes showed effective cell growth inhibition by triggering G0/G1 phase arrest and inducing apoptosis. FACScan results show remarkably high percentage of cell death induced by the complexes in the A549 cells, as compared to control. Annexin-V/PI staining of cells also indicated that the complexes induce cell death through the apoptotic pathway. The complexes are projected to be potential anticancer molecules that may interfere with DNA replication. This work makes a significant contribution to the virtually unknown chemistry of organometallic complexes as synthetic nucleases.

References

[1] T. W. Hambley, Dalton Trans., (2007) 4929.

[2] C. Orvig, M. Abrams, J.Chem. Rev., 99 (1999) 2201.

[3] K. H. Thompson, C. Orvig, Dalton Trans., (2006) 761.

[4] F. Arnesano, G. Natile, Coord. Chem. Rev., 253 (2009) 2070.

[5] Y. W. Jung, S. Lippard, J.Chem. Rev., 107 (2007) 1387.

[6] T.Boulikas, Pantos, A.; Bellis, E.; Christofis, P. Cancer Ther. 2007, 5, 537.

[7] S. van Zutphen, J. Reedijk, Coord. Chem. Rev., 249 (2005) 2845.

[8] R. Gust, W. Beck, G. Jaouen, H. Schoenenberger, Coord. Chem. Rev., 253 (2009) 2760.

[9] R. Gust, W. Beck, G. Jaouen, H. Schoenenberger, Coord. Chem. Rev., 253 (2009) 2742.

[10] P. C. A. Bruijnincx, P. J. Sadler, Curr. Opin. Chem. Biol., 12(2008)197.

[11] F. Tisato, C. Marzano, M. Porchia, M. Pellei, C. Santini, Med. Res. Rev., 30 (2010) 708.

[12] C. Marzano, M. Pellei, F. Tisato, C. Santini, Anti-Cancer Agents Med. Chem., 9 (2009) 185.

[13] S. Tardito, L. Marchio, Curr. Med. Chem., 16 (2009) 1325.

[14] T. Wang, Z. Guo, J.Curr. Med. Chem., 13 (2006) 525.

[15] C. Duncan, A. R. White, Metallomics., 2012, 4, 127.

[16] H. B. Kraatz, N. Metzler-Nolte, Concepts and Models in Bioinorganic Chemistry; Wiley-VCH: Weinheim, Germany, 2006.

[17] (a) M. F. R. Fouda, M. M. Abd-Elzaher, R.A. Abdelsamaia, A. A. Labib, Appl. Organomet. Chem. 21 (2007) 613

(b) C. S. Allardyce, A. Dorcier, C. Scolaro, P. Dyson, J.Appl. Organomet. Chem., 19 (2005) 1.

[18] M. Miwa, H. Tamura, Chem. Lett. (1997) 1177.

[19] B. Maity, M. Roy, A. R. Chakravarty, J. Organomet. Chem., 693(2007) 1395.

[20] (a) T. Moriuchi, T. Hirao, Top. Organomet. Chem., 17 (2006) 143.
(b) H.B. Kraatz, J. Inorg. Organomet. Polym. Mater., 15 (2005) 83.
(c) D.R. van Staveren, N. Metzler-Nolte, Chem. Rev., 104 (2004) 5931.

[21] L. Wang, A. Brock, B. Herberich, P.G. Schultz, Science., 292 (2001) 498.

[22] Z. Zhang, B. A. C. Smith, L.Wang, A. Brock,C. Cho, P.G. Schultz, Biochemistry., 42 (2003) 6735.

[23] J. W. Chin, T. A. Cropp, J. C. Anderson, M. Mukherji, Z. Zhang, P. G. Schultz, Science., 301(2003) 964.

[24] L. Alfonta, Z. Zhang, S. Uryu, J. A. Loo, P. G. Schultz, J. Am. Chem. Soc., 125 (2003) 14662.

[25] H. S. Lee, P. G. Schultz, J. Am. Chem. Soc., 130 (2008) 13194.

[26] D. R. Van Staveren, N. Metzler-Nolte, Chem. Rev., 104 (2004) 5931.

[27] A. Nguyen, S. Top, A.Vessieres, P. Pigeon, M. Huche, E. A. Hillard, G. Jaouen, J. Organomet. Chem., 692 (2007) 1219.

[28] C. Biot, G. Glorian, L. A. Maciejewski, J. S. Brocard, O. Domarle, G. Blampain, P. Millet, A. J. Georges, H. Abessolo, D. Dive, J.Lebibi, J. Med. Chem., 40 (1997) 3715.

[29] G.I. Miessler, D.A. Tarr, Inorganic Chemistry, third ed., Prentice Hall, (2003) 299.

[30] E. Meggers, Curr. Opin. Chem. Biol., 11 (2007) 287.

[31] J.K. Barton, Science., 233 (1986) 727.

[32] J.C. Francois, T. Saison-Behmoaras, M. Chassignol, N.T. Thuong, J.S. Sun, C. Helene, Biochemistry., 27 (1988) 2272.

[33] Q. Guo, M. Lu, N.C. Seeman, N.R. Kallenbach, Biochemistry., 29 (1990) 570.

[34] J.M. Kelly, A.B. Tossi, D.J. McConnell, Nucleic Acids Res., 13 (1985) 6017.

[35] G. Son, J. Yeo, M. Kim, S. Kim, A. Holmen, B. Akerman, B. Norden, J. Am. Chem.Soc., 120 (1998) 6451.

[36] S. Tabassum, W.M. Al–Asbahy, M. Afzal, F. Manalshamsi, Arjmand, J. Lumin., 132(2012) 3058.

[37] E.S. Koumousi, M. Zampakou, C.P. Raptopoulou, V. Psycharis, C.M. Beavers, S.J. Teat, G. Psomas, T.C. Stamatatos, Inorg. Chem., 51 (2012) 7699.

[38] C. Tolia, A.N. Papadopoulos, C.P. Raptopoulou, V. Psycharis, C. Garino, L. Salassa, G. Psomas, J. Inorg. Biochem., 123 (2013) 53.

[39] S. Dhar, M. Nethaji, A.R. Chakravarty, J. Inorg. Biochem., 99 (2005) 805–812.

[40] R.F. Pasternack, M. Cacca, B. Keogh, T.A. Stephenson, A.P. Williams, F.J. Gibbs, J.Am. Chem. Soc., 113 (1991) 6835.

[41] S. Eriksson, S.K. Kim, M. Kubista, B. Norden, Biochemistry., 32 (1993) 2987–2998.

[42] A. Biancardi, T. Biver, F. Secco, B. Mennucci, Phys. Chem. Chem. Phys., 15 (2013)4596.

[43] A.K. Williams, S.C. Dasilva, A. Bhatta, B. Rawal, M. Liu, E.A. Korobkova, Anal. Biochem., 422 (2012) 66–73.

[44] S. Satyanarayana, J.C. Dabrowiak, J.B. Chaires, Biochemistry., 32 (1993) 2573.

[45] D. Suh, J.B. Chaires, Bioorg. Med. Chem., 3 (1995) 723.

[46] C.J. Sherr, Cancer Res., 60 (2000) 3695.

[47] S.R. Umansky, B.A. Korol, P.A. Nelipovich, Biochim Biophys Acta., 655 (1981) 9.

[48] I. Vermes, C. Haanen, H. Steffens-Nakken, C .J. Reutelingsperger, Immunol Methods., 184 (1995) 39.